Figure 2. Typical sampling sites. (A) Bone River "best site".

composed of ring measurements from 18 trees.

6. Only one of the subfossil wood samples examined to date contains a marked change in ring widths representing the last, or nearly-last, few decades of tree growth. The general lack of changes in ring width among the last rings of most samples suggests that trees at all sites died rapidly, possibly within less than a year, following submergence of the roots of sampled trees below the level of high tide.

7. Samples collected from two of three modern sitka spruce stumps at the Grays River site show that these trees began growing before A.D. 1666 and 1668, respectively. These dates show that the modern forest at this site established at least 14 years before the A.D. 1682 and 1684 limiting dates we have inferred for submergence at the Copalis River and Chehalis River sites (Fig. 1).

Figure 2 (B). Johns River site. Redcedar snag is on right.

8. We are also in the process of revising FORTRAN program CORREL, a data-analysis computer program based on the approach of Yamaguchi (1986) for use in this project. CORREL computes correlation coefficients relating undated and control ring series at all possible positions of overlap.

E. <u>Discussion</u>: The 97-km spread of the eight subfossil redcedar sites is intriguing because <u>if</u> ongoing lab work shows that trees at these sites died synchronously, then the distribution of these sites implies that the earthquake that caused synchronous subsidence about 300 years ago was at least a magnitude 8 event (Atwater 1987). However, the geologic story that the subfossil redcedars record could be more complex than the synchronous coastal subsidence/massive tree-kill scenario we initially envisioned. The finding that modern sitka spruce began growing at the Grays River site before or during the A.D. 1660s shows that submergence may have occurred two decades

Figure 2 (C). Grays River/Malone Creek site.

earlier at this site than at the Copalis River and Chehalis River sites. Another possibility is that the synchronous-subsidence scenario is correct, but that forest succession at the Grays River site was controlled by factors other than coastal submergence. Further laboratory work is needed to distinguish between these possibilities.

F. Acknowledgments. The 1987-88 preliminary study was done while DKY was a National Research Council-USGS Research Associate at the Cascades Volcano Observatory, Vancouver, Washington. B. F. Atwater showed DKY the Copalis R., Chehalis R., Johns R., Niawiakum R., and Grays R. subfossil sites and the Long Island control site; K. A. Bevis helped with the field work. The 1988 field work was aided by J. E. Morales, and funded by a grant to INSTAAR's Center for Geochronological Research from the University of Colorado's Program Enrichment Fund. A. R. Nelson and D. W. Inouye reviewed the manuscript.

G. References.

Atwater, B.F. (1987). Evidence for great Holocene earthquakes along the outer coast of Washington state. Science 236, 942-944.

Fritts, H.C. (1976). Tree Rings and Climate. Academic Press, New York.

Heaton, T.H., and Hartzell, S.H. (1987). Earthquake hazards on the Cascadia subduction zone. Science 236, 162-168.

Reinhart, M.A., and Bourgeois, J. (1987). Distribution of anomalous sand at Willapa Bay, Washington: evidence for large-scale landward-directed processes. EOS 68, 1469.

Yamaguchi, D.K. (1986). Interpretation of cross correlation between tree-ring series. Tree-Ring Bulletin 46, 47-54.

H. Appendix. Descriptions and locations of redcedar sampling sites.

1. Copalis R.: Large number of redcedar snags standing on modern marsh (similar to Fig. 2A). Moclips quad., NW1/4 NE1/4 sec. 22, T. 19 N., R. 12 W. Many other snags available for sampling upstream.

2. Chehalis R.: Scattered redcedar snags standing in sitka spruce forest (similar to Fig. 2B); there are undoubtedly many more snags present than reported here. Central Park quad.
   a. Main channel Chehalis R.:
      (1) Two tall snags visible from channel in forest on south riverbank; SW1/4 NW1/4 and SE1/4 NW 1/4 sec. 19, T. 17 N., R. 8 W.
      (2) One snag on northwest riverbank at SW1/4 SW 1/4 sec. 17, T. 17 N., R. 8 W.
   b. N. Fk. of Preachers Slough: Four snags on slough banks in SE1/4 SW1/4 sec. 15, SW1/4 NW1/4 sec. 22 and NE1/4 NW1/4 sec. 22, T. 17 N. R. 8 W. Best local site found.

3. Johns R.: Scattered redcedar snags standing in sitka spruce forest on southwest riverbank (Fig. 2B). Hoquiam quad., SW1/4 SW1/4 sec. 8 and NW1/4 NW1/4 sec. 17, T. 16 N, R. 10 W.

4. Cedar R.: Redcedar snags standing on marsh surface on both banks of the Cedar R.'s east fork. Bay Center quad., NW1/4 SE1/4 sec. 31, T. 15 N., R. 10 W.

5. Bone R.: Redcedar snags standing on marsh surface on both banks of river; the best-preserved snags, including the one with intact bark, are on the southwest bank in Bay Center quad., SE1/4 NW1/4 sec. 35, T. 14 N, R. 10 W. (Fig. 2A). Other sampled trees are upstream in SE1/4 sec. 35, T. 14 N, R. 10 W.

6. Niawiakum R.: Many spruce root systems exposed in channel outcrops; one rotten logged redcedar stump also stands on the marsh surface. Nemah quad., W1/2 sec. 14, T. 13 N, R. 10 W.

7. S. Fk. Palix R.: Large number of logged redcedar stumps standing on marsh surface; similar to Fig. 2A. Most sampled stumps are in Nemah quad., SW1/4 NW1/4 sec. 35, T. 13 N., R. 10 W; see also NW1/4 NE1/4 sec. 34, and NW1/4 SW1/4 sec. 35.

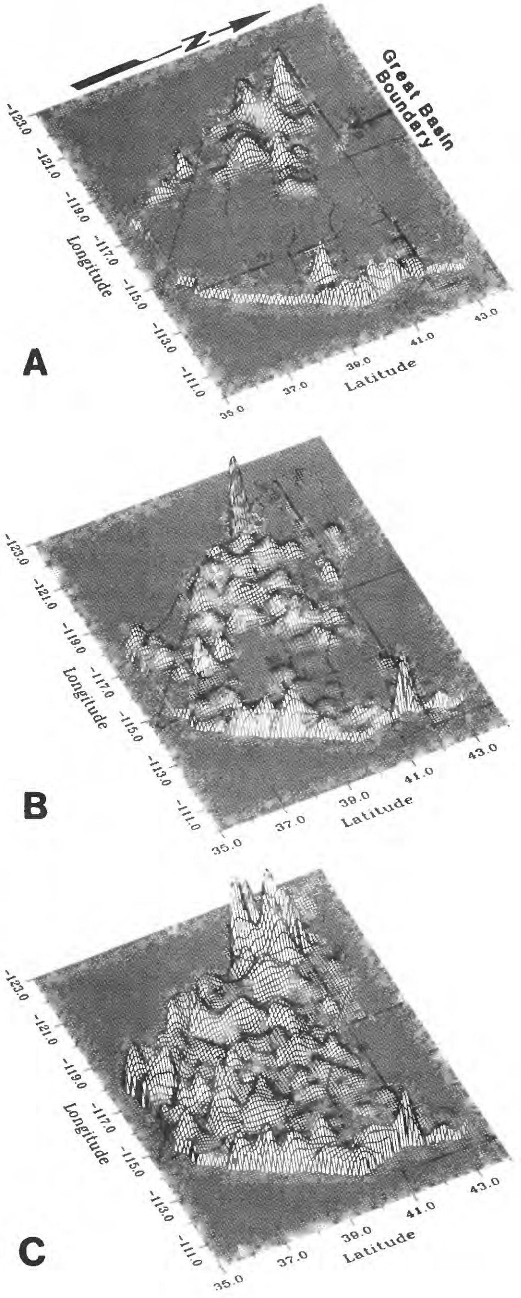

Figure 1. Relative density of A) Holocene and historic (post-pluvial, $\leq$0.012 m.y.), B) late Quaternary ($\leq$0.5 m.y.), C) all Quaternary surface faulting ($\leq$2 m.y.) in alluvium throughout the Great Basin normalized in terms of kilometers of surface rupture length per 625 km^2 (z-axis). West to northwest lines are trends of accommodation zones (transverse range-tilt boundary zones from Stewart, 1980).

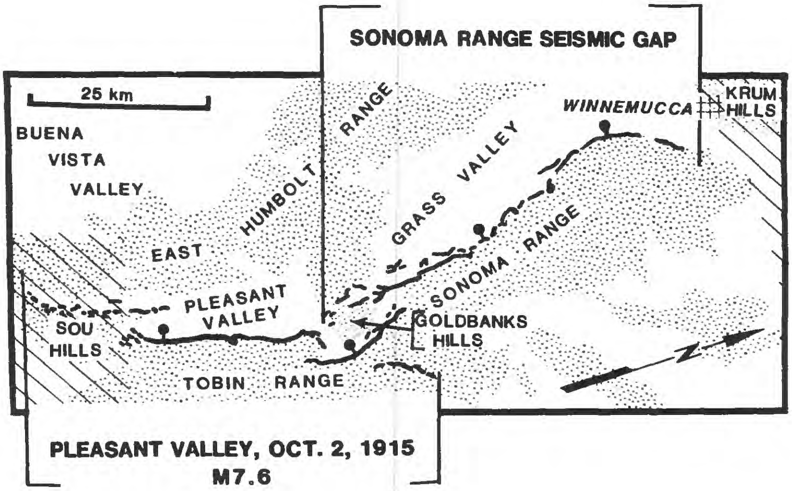

Figure 2. Map of surface faulting comprising the northern Central Nevada Seismic Zone showing ruptures of the October 2, 1915 Pleasant Valley earthquake and Holocene scarps comprising the Sonoma Range Seismic Gap. Ruled areas indicate approximate boundaries of the central and northern extensional accommodation zones where the zones cross the seismic belt at Sou Hills and Krum Hill, respectively.

Regional and Local Hazards Mapping in the Eastern Great Basin*

9950-01738

R. Ernest Anderson
Branch of Geologic Risk Assessment
U.S. Geological Survey
Box 25046, MS 966, Denver Federal center
Denver, CO 80225
(303) 236-1584

*Without changing the name of the project it has been expanded to include a major component of study by G.C.P. King of Methods of Assessing local and Regional Seismic Hazards.

Investigations

1. Assembled and analyzed from varied sources geologic evidence for north-south constrictional strain of late Cenozoic age in the southern Great Basin.

2. Developed methods and the necessary computer programs to model geological structures and morphological features associated with active dip-slip and strike-slip faults. A specific purpose of this work is to allow general features of the geology and landscape to be used to assess rates of fault motion and hence add to the tools available to assess seismic hazard. The work is also of fundamental importance to understanding strain distributions associated with active faults.

3. Developed methods and the necessary programs to express seismicity maps in terms of contour maps of slip distribution. Combined with geodetic data, this will allow the traditional methods of using b-values to assess seismic hazard to be placed on a more solid physical basis.

Results

1. The common occurrence of strike-slip focal mechanisms from widely distributed areas in the Great Basin has yet to be explained in terms of a unifying tectonic model because there is a general lack of geologic fault-slip data consistent with the orientation and slip characteristics inferred from the earthquake record. There are within and directly south of the southern Nevada seismic belt many fault and fold structures of widely varying scale that are broadly consistent with regional north-south late Cenozoic constrictional strain. We have assembled and begun to analyze data pertaining to these structures and have determined numerous localities from which additional data on the architecture and kinematics are needed and will be gathered as part of an effort to understand whether or not these structures are compatible with the earthquake record.

2. The geological structures associated with the White Wolf fault (1975, Kern County earthquake), the Lost River fault (1985, Borah Peak earthquake), and the Cricket Mountain fault have been modeled using methods previously used only to model the seismic cycle (King and others, 1988; Stein and

others, 1988). It has been shown that the assumption that earthquakes repeat on the same fault can be used to predict the form of geological structures. This means that geological features can be used to assess seismic hazard without the need (necessarily) to trench surface faults. In the case of reverse-faulting environments, faults can be hard or impossible to locate; hence, the techniques under development are of particular importance. The Los Angeles basin is a prime candidate for application of the methods being developed.

The structures around strike-slip faults also provide information about fault rates and the technique has been applied in the Parkfield and Coachella Valley regions of California (Bilham and King, 1989; Shedlock and others, 1989). Preliminary work has also been carried out on the northern San Andreas (Point Reyes region).

The work so far has emphasized seismic hazard but other hazards can arise from progressive tectonic deformation. John Whitney (USGS Western Regional Geology) has shown that the Ganges delta of Bangla Desh is undergoing active deformation because of its location above a wrench fault system. The vertical motions apparently control the long-term course of the rivers. This view has important implications. It means that flooding is triggered and not caused by weather. Building levees must fault in the long term. River management based on a proper understanding of the tectonics will provide a realistic solution. Similar problems exist in other parts of the world including the United States. For example, the creation of the Salton Sea by the diversion of the Colorado River resulted from elevation changes caused by tectonics. In this case, the trigger for change was the Army Corps of Engineers and not the weather. The methods of tectonic modeling being developed for seismic-hazard purposes are ideally suited to these problems.

3. It has been customary in seismic-hazard evaluation to look at seismic hypocenter distribution, energy release and so forth. Commonly the hazard from large earthquakes is predicted on the assumption that the Gutenberg-Richter relationship may be extrapolated from small to large magnitudes. Other methods of establishing hazard depend on studying fault slip or geodetic deformation. Bakun and others (1984) and King and Bakun (1986), however, showed that geodetic slip, fault slip, and seismic slip can be compared directly in terms of a slip budget. The important step was to establish earthquake moments and convert this to slip, and the method was tested for a region of the Calaveras fault in California with a primary emphasis on understanding fault mechanics. The early computer programs that King and Bakun developed are now being modified to suit them to more general seismic-hazard purposes.

Reports

King, G.C.P., Stein, Ross, and Rundle, J., 1988, The growth of geological structures by repeated earthquake--Conceptual framework: Journal of Geophysical Research, v. 93, no. B11, p. 13307-13318.

Stein, Ross, King, G.C.P., and Rundle, J., 1988, The growth of geological structures by repeated earthquakes--Field examples of continental dip-slip faults: Journal of Geophysical Research, v. 93, no. B11, 13319-13331.

Anderson, R.E., and Christenson, G.E., 1989, Quaternary faults and potential for surface-faulting earthquakes, southwestern Utah: Geological Society of America Abstracts with Programs, v. 21, no. 5, p. 50-51.

Bilham, R.G., and King, G.C.P., 1989. The morphology of strike slip faults; examples from the San Andreas: Journal of Geophysical Research. (In press.)

King, G.C.P., Sturdy, D., and Whitney, J., Landscape geometry and active tectonics of northwest Greece. (In preparation.)

Strong Motion in San Bernadino and Riverside Counties from a Moderate Earthquake on the San Jacinto Fault

14-08-001-G1689

Ralph J. Archuleta
Institute for Crustal Studies and Department of Geological Sciences
University of California, Santa Barbara
Santa Barbara, CA 93106
(805) 961-4477

Objectives: The objective of this project is to compute strong ground motion at selected sites within 25 km of the northern San Jacinto fault assuming a moderate earthquake on this section. The earthquake source model is a spontaneously propagating stress relaxation on an inhomogeneously stressed fault. The dynamics of the rupture are modeled using a 3-D finite element code by which the slip rate is determined at a grid of points on the fault. The slip rate is convolved with numerical Green's functions computed from a discrete wavenumber/finite element code and integrated over the fault to produce strong motion at sites off the fault. The critical element, and admittedly ad hoc, is the specification of the distribution of stress inhomogeneity on the fault. Our approach is to consider other faults that intersect the San Jacinto (Figure 1) and the seismicity pattern on the San Jacinto fault (Figure 2). Our assumption is that areas of the San Jacinto fault where other faults intersect and/or regions where the seismicity is low have higher yield stress than other parts of the fault.

Results: This project was started in January 1989. We have started to develop the spontaneous rupture code based on a previous code for simulating a propagating rupture with a specified rupture velocity. The data showing location of intersecting faults and seismicity has been collected. Strong motion data to be used to constrain the model are not yet available.

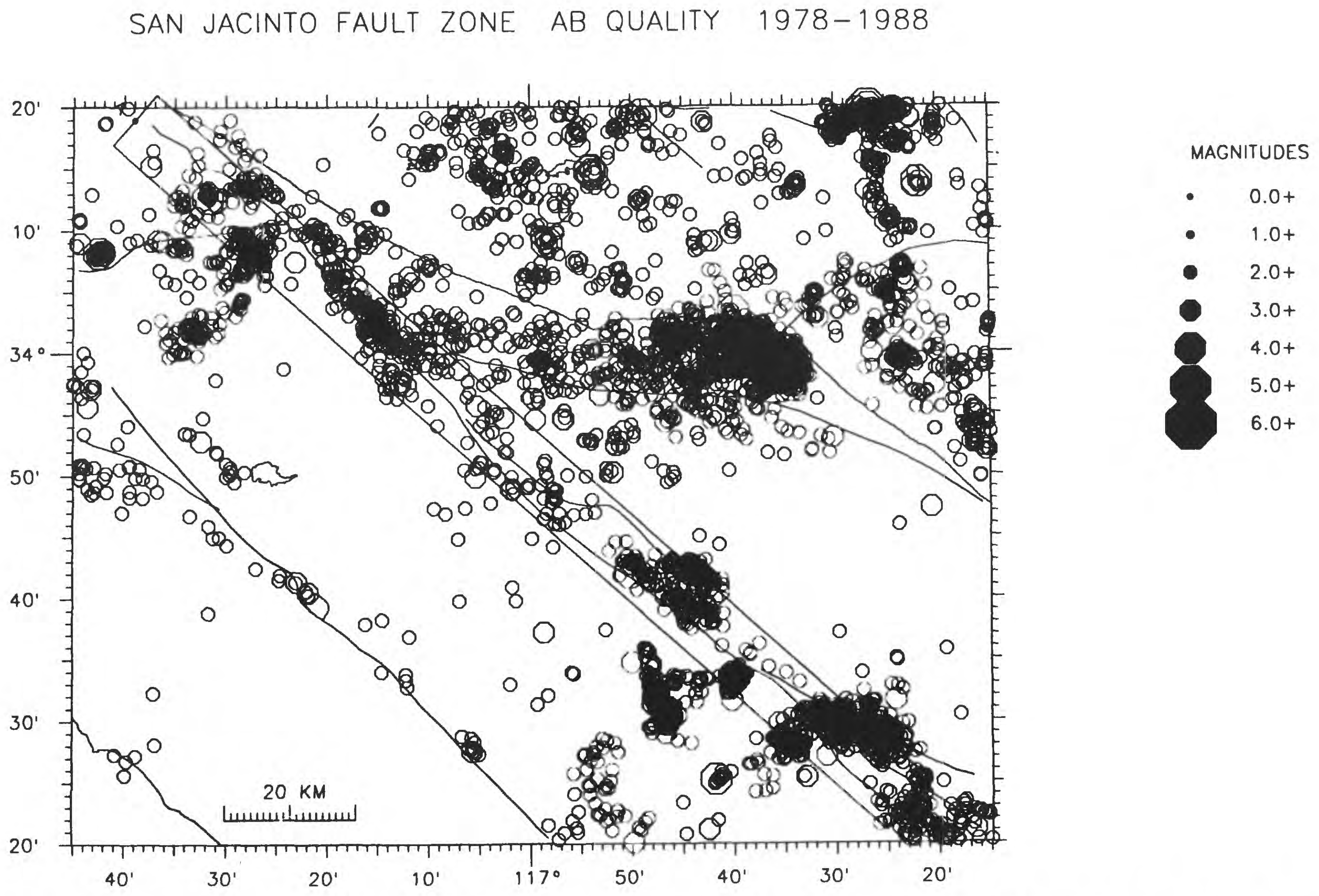

Figure 1. Plan view of the San Jacinto fault showing epicenters (M > 2) and major faults in the region. The rectangular box (from 34° 19' N, 117° 39' W (A) to 33° 23' N, 116° 23' W (A')) is used to make the cross section shown in Figure 2.

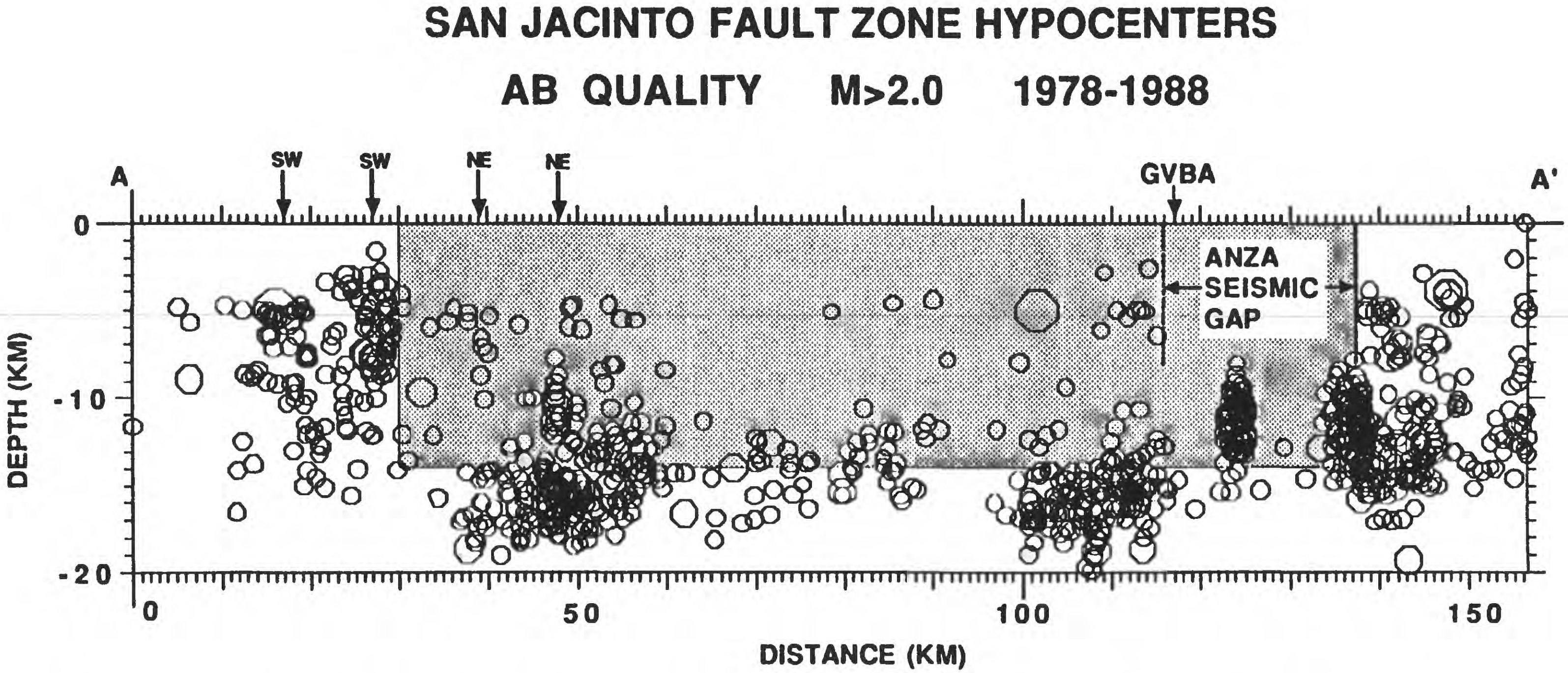

Figure 2. Cross section of the San Jacinto fault from its intersection with the San Andreas to the region 18 km south of the Anza seismic gap. Seismicity within ± 5 km of the San Jacinto is projected onto the plane. Although the epicenters indicate nearly uniform seismicity along strike on the northern San Jacinto, the hypocenters show that the seismicity is primarily confined to depths between 13-18 km leaving a large areas on the fault with little seismicity.